Attenuation surface noise with autoencoders

Ivan J. Sánchez-Galvis *, Daniel O. Trad†, William Agudelo‡ and Daniel Sierra*,

ABSTRACT

Surface wave attenuation is one of the essential stages in data processing for land seismic exploration. Conventionally, this stage involves $f-k$ filters that can separate the surface waves in a specific area of frequency and wavenumber domain. However, these filters must be tuned manually shot by shot according to the surface wave behavior in the acquisition zone. Thus the quality of the filtered data depends on human expertise, and processing times increase according to the number of shots. Moreover, the $f-k$ filter requires seismic data with uniform spatial sampling, which is not possible in some complex land area acquisitions. Therefore, we propose to use a convolutional autoencoder to predict the Radon model of seismic data without surface wave noise. The Radon model allows working with seismic data with irregular spatial sampling. We train the autoencoder with synthetic data generated by elastic wave modeling with several 2D earth models. The results show that the trained model can accurately attenuate the surface noise with a performance similar to well-tuned $f-k$ filters.

INTRODUCTION

The $f-k$ filter is the most widely used method to remove ground roll. Although this method presents two big limitations when data acquired in land complex areas need to be processed. The first of them is that the $f-k$ filter requires to have data regularly sampled in both, time and offset (Yilmaz 2001). However, in complex land areas is not possible to ensure seismic acquisitions with the same interval distance for all the receivers in a line. To arise this problem, some methods based on the Linear Radon Transform (LRT) have been proposed (Luo et al. 2009; Hu et al. 2016). These methods can accurately remove the surface waves in the $f-v$ (frequency-velocity) domain estimated from the seismic shot gather, which does not need to be regularly sampled in offset (Trad et al. 2003). The second big limitation of the $f-k$ filter is those body wave events that overlap with the surface noise in the $f-k$ domain could be attenuated by the filter. Therefore, additional characteristics must be included to find patterns that differentiate surface waves from body waves. For instance, polarization is elliptical for the surface waves and linear for the body waves. In the literature, it is possible to find several polarization filters to attenuate ground roll (de Franco and Musacchio 2001; Kendall et al. 2005; de Meersman and Kendall 2005; Pinnegar (2006); Sánchez-Galvis et al. 2016). Nevertheless, it is necessary to have multicomponent data to measure polarization, but they are not available for most cases.

In the last ten years, the usage of machine learning algorithms in geophysical applications have been rapidly increased. These algorithms are used to train models to find patterns within example datasets automatically. Applications in Geophysics include seis-

*Universidad Industrial de Santander
‡Centro de Innovación y Tecnología - ECOPETROL S.A.
‡CREWES - University of Calgary

mic facies classification (Zhao et al. 2015; Wrona et al. 2018; Puzyrev and Elders 2022), faults detection (Wu et al. 2019; Wang et al. 2020b; An et al. 2021), geophysical inversion (Zheng et al. 2019; Russell 2019; Chen and Schuster 2020), first arrival picking (Hu et al. 2019; Tsai et al. 2019) , seismic trace interpolation (Mandelli et al. 2018; Wang et al. 2020a) , among others. In this work, we propose a machine learning workflow to attenuate surface wave noise in seismic shot gathers. The workflow includes an Unet autoencoder to predict the Radon model of seismic data without surface noise. The Unet was trained with synthetic data obtained by using a solver for 2D elastic wave modeling, which can generate data with and without surface noise. The results show that the proposed workflow can accurately remove the surface waves with a similar performance to a well-tuned $f-k$ filter.

METHOD

Linear Radon Transform

The forward linear Radon Transform (LRT) in the frequency domain is given by (Yilmaz 2001):

$$d(h,f) = \sum_{p=p_{\text{min}}}^{p_{\text{max}}} m(p,f)\exp(i2\pi fph) \tag{1}$$

and the adjoint transformation,

$$m(p,f) = \sum_{h=h_{\text{min}}}^{h_{\text{max}}} d(h,f)\exp(-i2\pi fph) \tag{2}$$

where $d(h,f)$ is the shot gather after the temporal Fourier transform, the function $m(p,f)$ is the Radon model, f is the frequency, p is the slowness (p_{min} and p_{max} are the slowness range), and h is the offset (h_{min} and h_{max} are the slowness range).

The LRT can be written in a matrix form as follows:

$$\mathbf{d} = \mathbf{L}\mathbf{m} \tag{3}$$

where $\mathbf{d}$ and $\mathbf{m}$ are vectors that represent the shot gather and the Radon model in a slice of frequency, respectively. The operator $\mathbf{L} = \exp(i2\pi fph)$ is a complex matrix of $n_h \times n_p$, where n_h is the number of offsets, and n_p is the number of slowness.

The adjoint transformation can be also written in a matrix form:

$$\mathbf{m}_{\text{adj}} = \mathbf{d} \tag{4}$$

where $\mathbf{L}^{\mathrm{H}}$ is the conjugate transpose of $\mathbf{L}$, and $\mathbf{m}_{\mathrm{adj}}$ is the adjoint Radon model. This adjoint model has low resolution and it cannot be used to reconstruct the original data. However, the inverse LRT (also known as High Resolution LRT) is used to find the Radon model that best fits the data by using an inversion scheme with sparsity constraint (Trad et al. 2003; Luo et al. 2009). Figure 1 shows an example of application of the LRT on seismic data. In this example, the inverse LRT is used to estimate the Radon model in the frequency-slowness domain, and then the seismic data are reconstructed back by using the forward LRT.

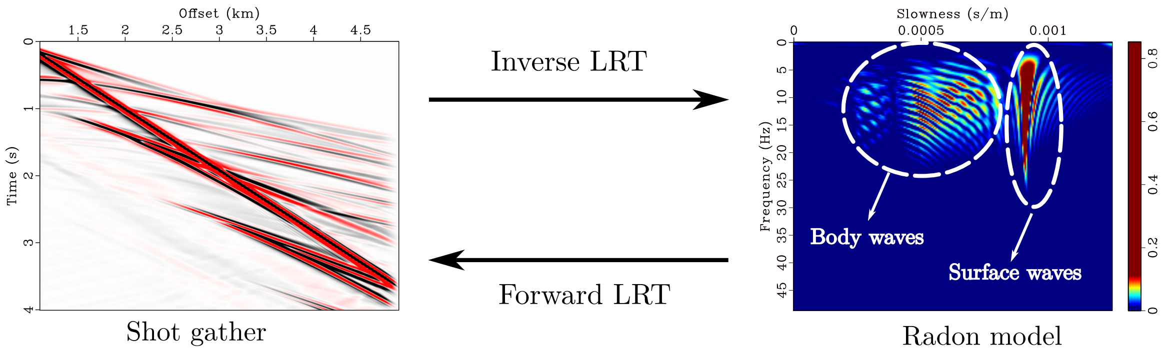

FIG. 1. Aplication of the LRT on seismic data. The inverse LRT is used to estimate the Radon model (right) from the shot gather (left). The Radon model allows to identify the zones of body and surface waves in the frequency-slowness domain. The seismic shot gather is reconstructed by applying the forward LRT.

Unet autoencoder

Convolutional Neural Networks (CNNs) is a type of Artificial Neural Network (ANNs) mainly used to image and video processing applications. These networks use convolutional kernels to extract feature maps from the input image. The feature maps are pooled to reduce the dimension of each resulting map that is used as the input of a fully connected ANN. Therefore, CNNs don't need to receive the features of each example as input because they can extract and select the most representative features directly from the raw image.

Convolutional autoencoders are a kind of CNNs that can learn dense representations of the input data (Géron 2022). The autoencoder is divided into two parts, the encoder and the decoder. The encoder is composed of convolutional and pooling layers that convert the input data to a latent representation with lower dimensionality. The decoder uses upsampling layers with convolutional layers to reconstruct the output that best fits the input data. This encoding-decoding process forces the autoencoder to find an internal representation with the most representative features in the input data.

Unet is a convolutional autoencoder architecture designed for biomedical segmentation applications (Ronneberger et al. 2015). In the decoder part, feature maps produced by the encoder are added after upsampling layers to propagate context information to higher-resolution layers. Before feeding the network, a tiling strategy is applied to train large images to produce patches with lower dimensions. This strategy allows Unet can yield precise segmentations with very few training images cause training data in terms of patches is much larger than the number of training images.

Figure 2 shows the Unet architecture used to predict the Radon model of seismic shot gathers without surface wave noise. The input must be a 64×64 2D data array that is coded in four levels including five 3×3 convolutional layers and four 2×2 max-pooling layers. The latent representation is decoded by five 3×3 convolutional layers and four 2×2 up-pooling layers. In the decoding, the output of each level of decoding is copied and cropped in each level of decoding. The resulting image is passed through a 1×1 convolutional layer with a $\tanh$ activation function.

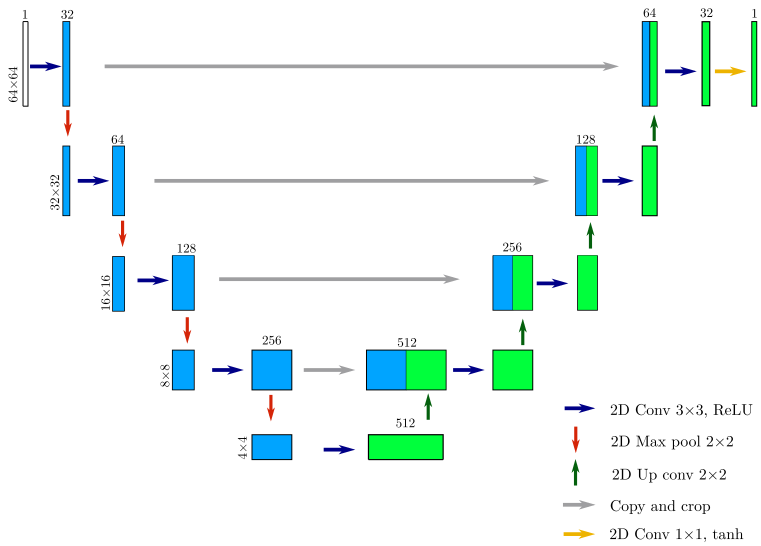

FIG. 2. Unet architecture used to predict the Radon model of seismic shot gathers without surface wave noise. This network has four levels of coding to find the latent representation of a 64×64 2D data array.

Workflow

The method to attenuate the surface wave noise in seismic shot gathers is divided into two parts. The first part consists of training the Unet convolutional autoencoder to predict the Radon model of seismic data without surface waves. In the training process, the input and label are the Radon model of the seismic data with and without surface wave noise, respectively. The second part is using the trained Unet in a workflow to attenuate the surface wave noise in seismic shot gathers, see Figure 3. The trained Unet predicts the Radon model without the surface wave energy, and subsequently, the filtered shot gather is computed by using the forward LRT.

NUMERICAL TEST

We tested the proposed method in a synthetic example. Figure 4 shows the reference earth model used to generate synthetic data with a 2D elastic wave modeling solver. Synthetic shot gathers were generated with 100 different versions of the earth model, where the S-wave velocity in the first layer ranges from 1000 to 1800 (m/s) in steps of 8 (m/s). For each model version, we performed two different modelings. In the first model, we solve the elastic wave equation with the two layers model to produce surface waves and body wave reflections and refractions. In the second model, we solve the elastic wave equation with only the first layer of the model to produce only surface waves. Thus, we can generate syn-

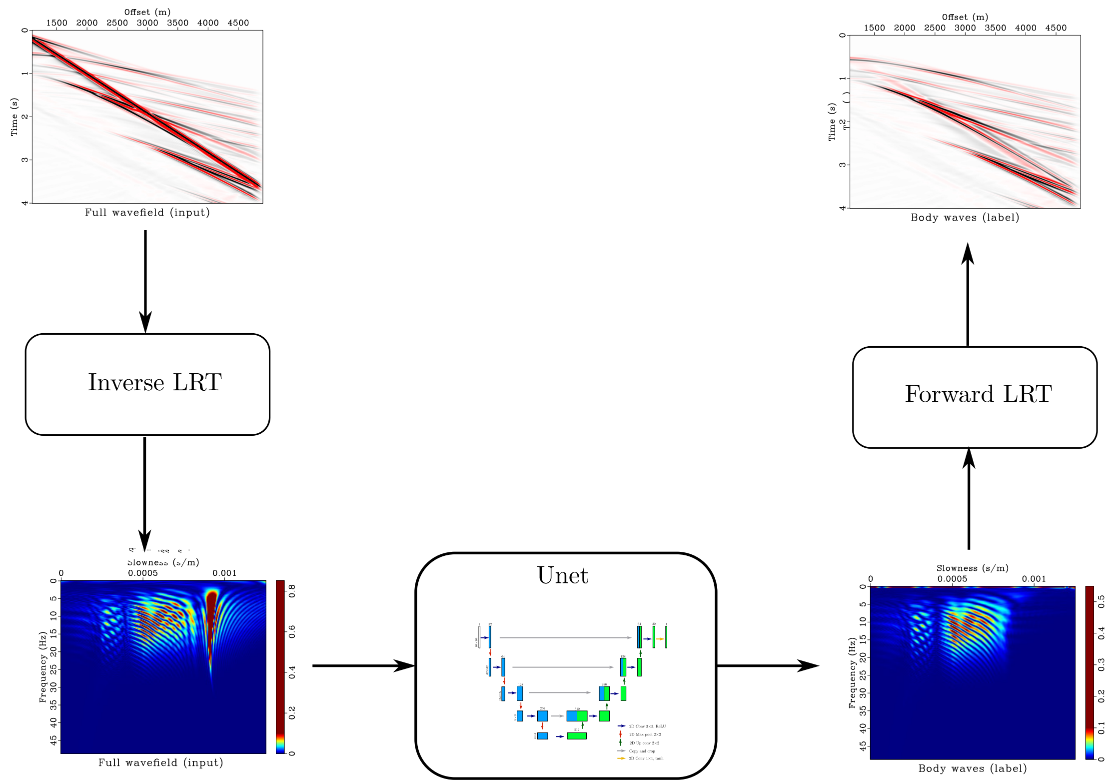

FIG. 3. Proposed workflow to attenuate the surface wave noise in seismic data. The Radon model of the raw shot gather is the input of the Unet model. The output is the Radon model containing just the body wave information. The shot gather without surface wave noise are obtained by computing the Forward LRT of the predicted Radon model

thetic data without surface wave noise by subtracting the resulting data from each model. In every shot gather, the source was a 10 Hz Ricker wavelet located at 10 (m) depth and 100 (m) horizontal distance, and the receivers were located on the surface from 1100 (m) to 4800 (m) horizontal distance with 10 (m) of interval.

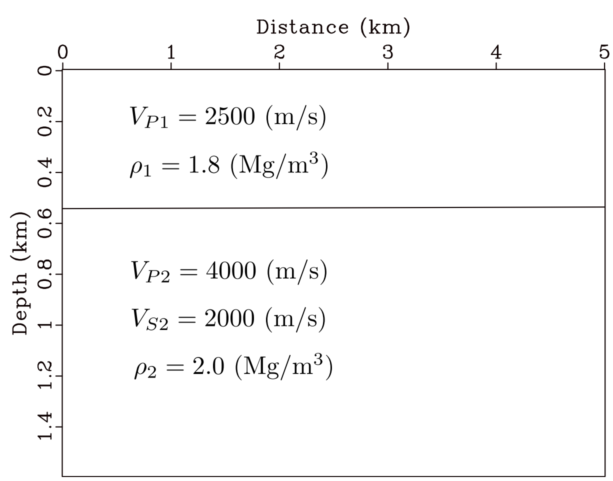

FIG. 4. 2D elastic model used to generate the synthetic data. The source location is at 10 m depth and 100 m of horizontal distance. The receivers are located on the surface from 1100 m to 4800 m of horizontal distance with 10 m of interval. Different acquisition were performed by varying the S-wave velocity in the first layer, which ranges from 1000 to 1800 (m/s) in steps of 8 (m/s).

Figure 5 shows one example of the shot gathers of the synthetic dataset. The shot gather in Figure 5a is the recorded full wavefield generated with the model of two layers. On the other hand, Figure 5a shows the shot gather of the surface waves generated with the model of only the top layer. By subtracting these two shot gathers, it is possible to get the shot gather of body waves without surface noise in Figure 5c. The Radon models of each shot gathers are shown in Figures 5d, 5e, and 5f. We observe that the surface noise is easily separated from the body waves in the Radon panel.

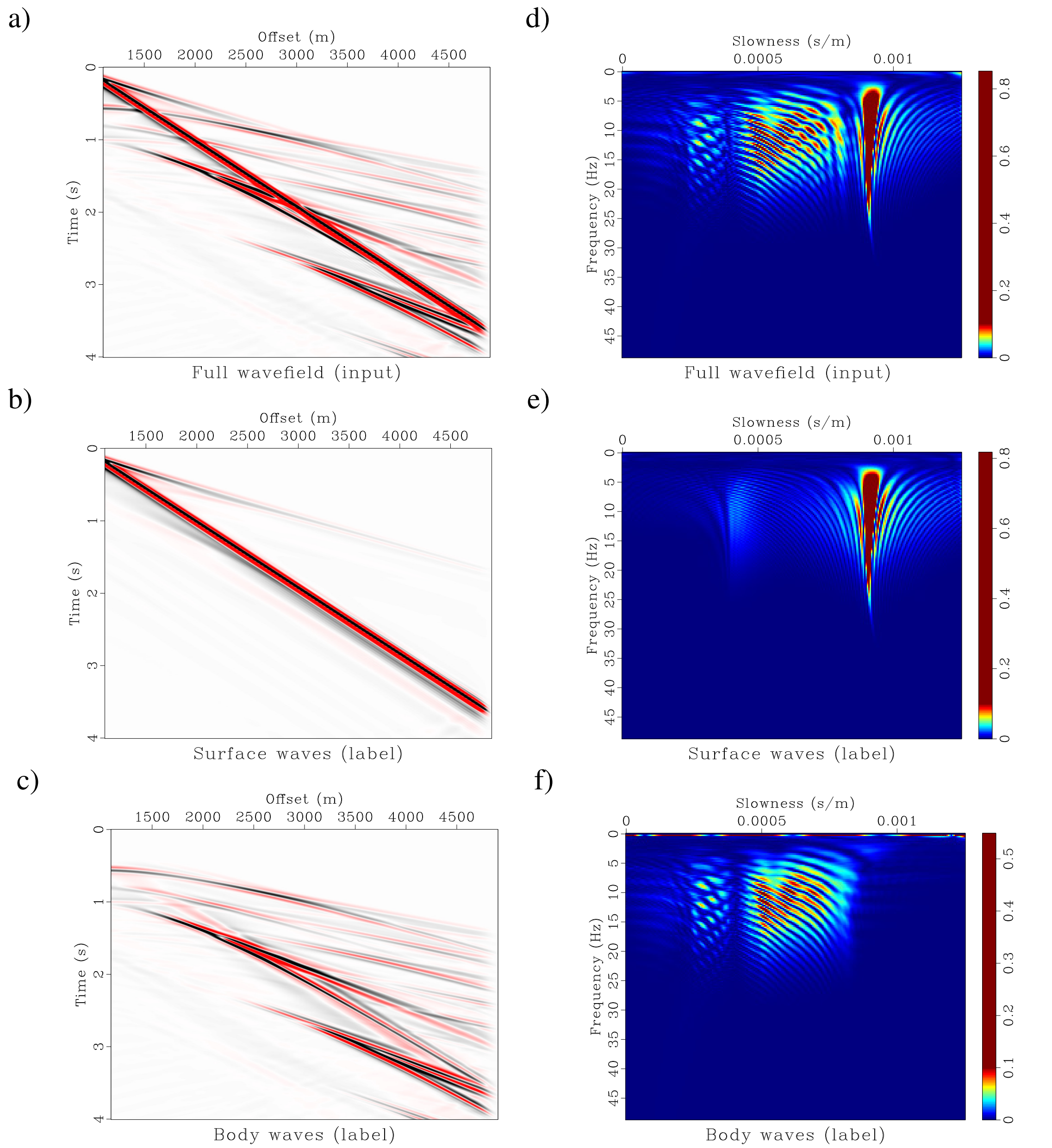

FIG. 5. Example of synthetic shot gather acquired with the model in Figure 4. Three different data are obtained by modeling. a) Full-wavefield data (body waves and surface waves), b) Surface waves, and c) Body waves (difference between a) and b)). The Radon models in d, e), and f) correpond to the data for the full-wavefield, surface waves and body waves, respectively.

We trained the Unet using the Radon model of the full wavefield and the body waves as input and label, respectively. In the training process, we used 80% of the dataset to train and the resulting 20% to validate. Figure 6 shows the learning curve of the Unet for training and validation in 40 epochs. We note that the training MSE decreases considerably in the first epochs and the knee effect is between 5 and 10 epochs. Similarly, the validation MSE decreases in the first epochs and fluctuates in the same range of values after 10 epochs.

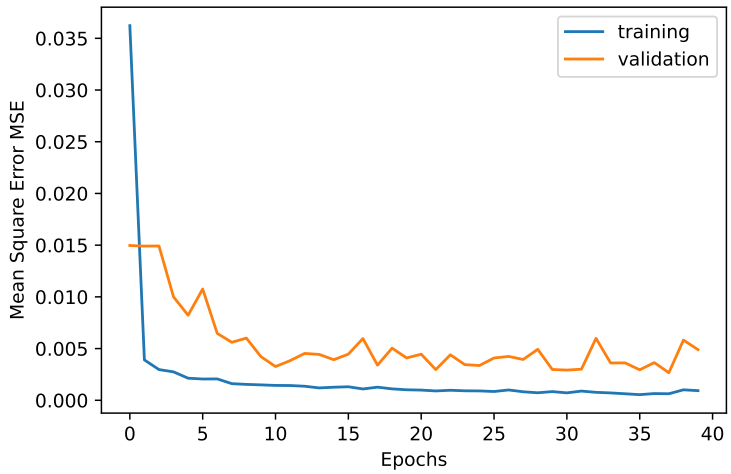

FIG. 6. Mean square error of predictions for training and validation according to the number of epochs.

Figure 7 shows an example of prediction performed by the trained Unet model. We observe that the Unet can accurately predict the Radon model without the surface noise energy. The free-noise shot gather is reconstructed by using the forward LRT.

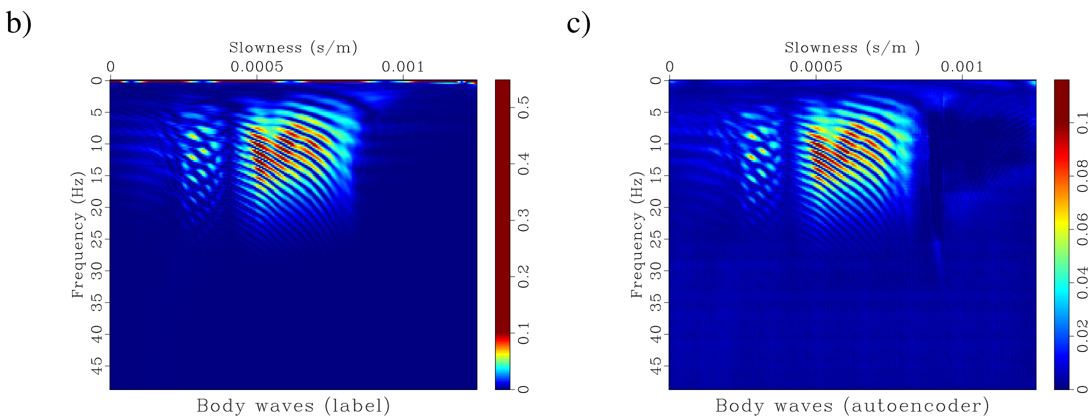

FIG. 7. Comparison of a Radon model example of body waves. a) True model .b) Predicted model by Unet.

We compared the surface noise attenuation performed by the Unet autoencoder with the $f-k$ filter. Figure 8 shows the shot gather of body and surface waves extracted by these methods. By comparing with the modeled shot gathers, we can say that the $f-k$ filter produces more clear events but is more aggressive than the Unet autoencoder. From the resulting shot gathers, it is observed that the $f-k$ filter attenuated two body wave events that the proposed workflow was able to preserve (events A and B in Figures 8b and 8c). Looking at the shot gathers of surface waves, we noted that those body wave events propagate close to the velocity of the Rayleigh wave. Thus the $f-k$ filter could not differentiate them. It is also noticeable that the predicted data with the Unet autoencoder exhibits some background artifact events produced by the Radon transformation. We believe that those noisy events can be attenuated by using a matching filter where only the events correlated with the raw data would be reconstructed.

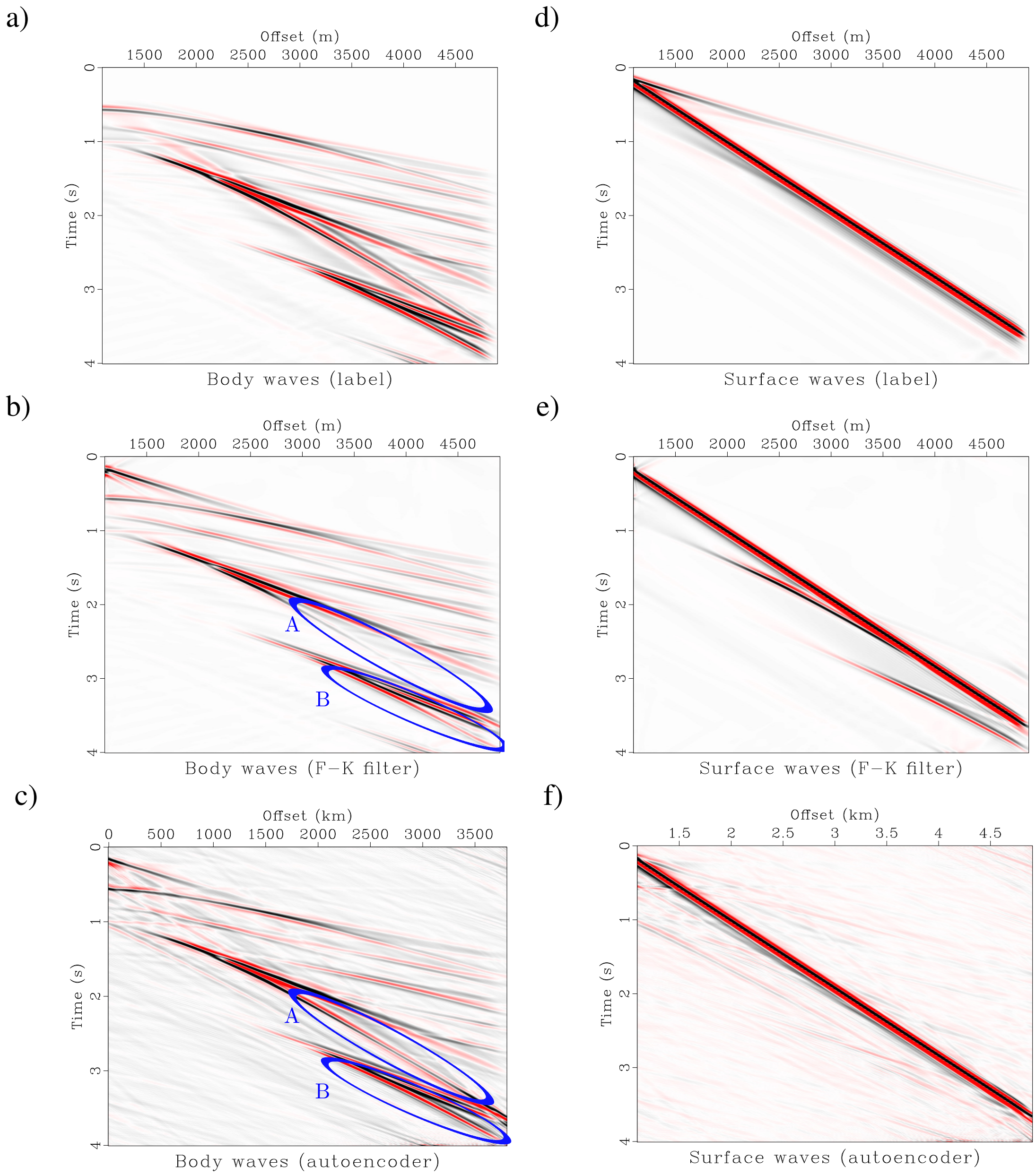

FIG. 8. Shot gathers with predicted body and surface waves. a) Modeled body waves. b) Body waves extracted by $f - k$ filter. c) Body waves predicted by the Unet model. d) Modeled surface waves. e) Surface waves extracted by $f - k$ filter. f) Surface waves predicted by the Unet model.

Finally, we compared the result of the surface noise attenuation in the $f - k$ domain. Figure 9 shows the $f - k$ spectra of the example shot gather in Figures 5 and 8. We can easily identify the energy of the surface and body wave in the spectrum of the modeled full wavefield (Figure 9a). The $f - k$ spectrum of the modeled body waves is displayed in Figure 9b. This spectrum is used as a gold standard to evaluate the filtering performance.

Figure 9c and 9d show the spectrum of the body waves extracted by the $f - k$ filter and predicted by the Unet autoencoder, respectively. We observe that the data predicted by the Unet are more accurate than the data obtained by the $f - k$ filter. Therefore, the proposed workflow becomes a good alternative to attenuate surface wave noise.

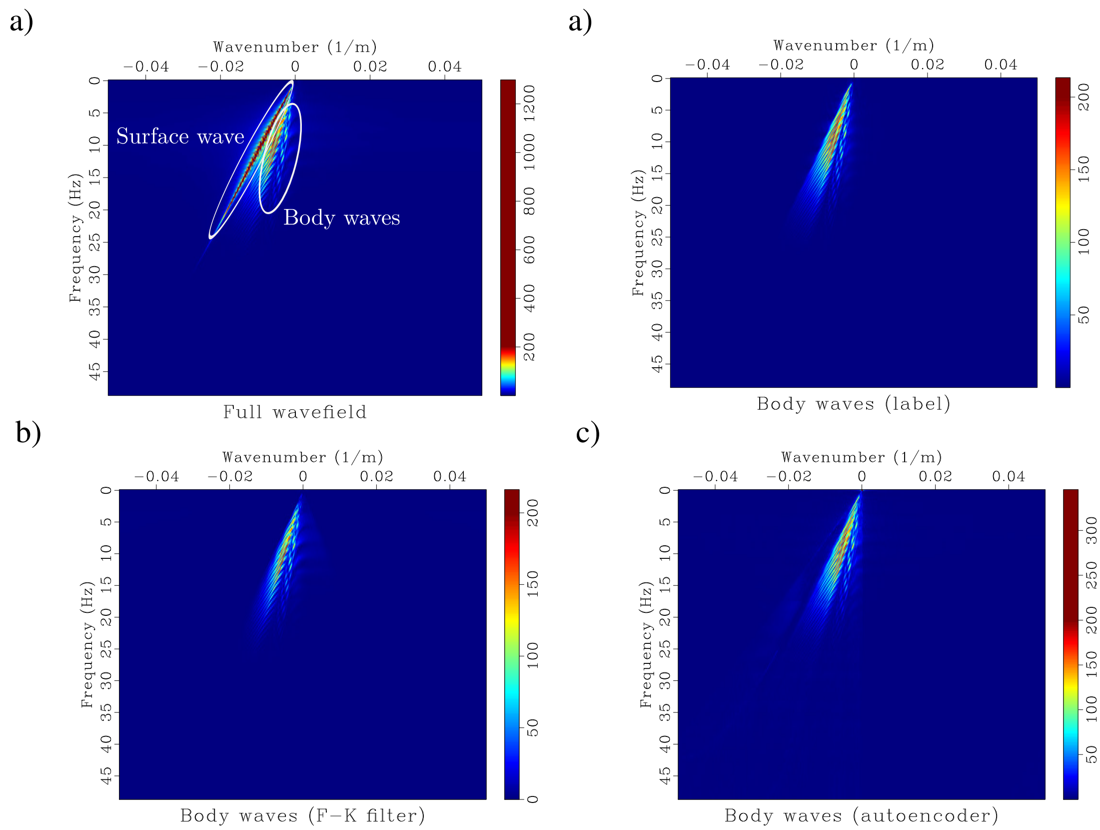

FIG. 9. Spectra of predicted body waves in the $f - k$ domain. a) Modeled full wavefield. b) Modeled body waves. c) Body waves extracted by $f - k$ filter. d) Body waves predicted by the Unet autoencoder.

CONCLUSIONS

We have presented a machine learning workflow to attenuate surface wave noise in seismic shot gathers. The workflow uses an Unet autoencoder to predict the Radon model of seismic data without surface noise. The Unet was trained with synthetic data generated by elastic wave modeling with several versions of the same 2D earth model. The performance of the proposed workflow was compared with a well-tuned $f - k$ filter in both, the $t - x$ domain, and the $f - k$ domain. The results showed that the proposed workflow can accurately remove the surface waves by preserving more energy of body waves than the $f - k$ filter. However, some background artifacts are produced by the Radon transformation. Therefore, we conclude that the proposed workflow becomes a good alternative to attenuate surface wave noise with a performance similar to well-tuned $f - k$ filters.

REFERENCES

An, Y., Guo, J., Ye, Q., Childs, C., Walsh, J., and Dong, R., 2021, Deep convolutional neural network for automatic fault recognition from 3d seismic datasets: Computers & Geosciences, **153**, 104,776.

Chen, Y., and Schuster, G. T., 2020, Seismic inversion by newtonian machine learning: Geophysics, **85**, No. 4, WA185–WA200.

de Franco, R., and Musacchio, G., 2001, Polarization filter with singular value decomposition: Geophysics, **66**, No. 3, 932–938.

de Meersman, K., and Kendall, R., 2005, A complex svd-polarization filter for ground roll attenuation on multi-component data, *in* 67th EAGE Conference & Exhibition, European Association of Geoscientists & Engineers, cp–1.

Géron, A., 2022, Hands-on machine learning with Scikit-Learn, Keras, and TensorFlow: " O'Reilly Media, Inc.".

Hu, L., Zheng, X., Duan, Y., Yan, X., Hu, Y., and Zhang, X., 2019, First-arrival picking with a u-net convolutional network: Geophysics, **84**, No. 6, U45–U57.

Hu, Y., Wang, L., Cheng, F., Luo, Y., Shen, C., and Mi, B., 2016, Ground-roll noise extraction and suppression using high-resolution linear radon transform: Journal of Applied Geophysics, **128**, 8–17.

Kendall, R., Jin, S., Ronen, S., and De Meersman, K., 2005, An svd-polarization filter for ground roll attenuation on multicomponent data, *in* SEG Technical Program Expanded Abstracts 2005, Society of Exploration Geophysicists, 928–931.

Luo, Y., Xia, J., Miller, R. D., Xu, Y., Liu, J., and Liu, Q., 2009, Rayleigh-wave mode separation by high-resolution linear radon transform: Geophysical Journal International, **179**, No. 1, 254–264.

Mandelli, S., Borra, F., Lipari, V., Bestagini, P., Sarti, A., and Tubaro, S., 2018, Seismic data interpolation through convolutional autoencoder, *in* SEG Technical Program Expanded Abstracts 2018, Society of Exploration Geophysicists, 4101–4105.

Pinnegar, C., 2006, Polarization analysis and polarization filtering of three-component signals with the time—frequency s transform: Geophysical Journal International, **165**, No. 2, 596–606.

Puzyrev, V., and Elders, C., 2022, Unsupervised seismic facies classification using deep convolutional autoencoder: Geophysics, **87**, No. 4, 1–39.

Ronneberger, O., Fischer, P., and Brox, T., 2015, U-net: Convolutional networks for biomedical image segmentation, *in* International Conference on Medical image computing and computer-assisted intervention, Springer, 234–241.

Russell, B., 2019, Machine learning and geophysical inversion—a numerical study: The Leading Edge, **38**, No. 7, 512–519.

Sánchez-Galvis, I.-J., Serrano-Luna, J.-O., Niño-Niño, C.-A., Sierra, D.-A., and Agudelo-Zambrano, W.-M., 2016, Svd polarization filter taking into account the planarity of ground roll energy: CT&F-Ciencia, Tecnología y Futuro, **6**, No. 3, 5–24.

Trad, D., Ulrych, T., and Sacchi, M., 2003, Latest views of the sparse radon transform: Geophysics, **68**, No. 1, 386–399.

Tsai, K. C., Hu, W., Wu, X., Chen, J., and Han, Z., 2019, Automatic first arrival picking via deep learning with human interactive learning: IEEE Transactions on Geoscience and Remote Sensing, **58**, No. 2, 1380–1391.

Wang, Y., Wang, B., Tu, N., and Geng, J., 2020a, Seismic trace interpolation for irregularly spatial sampled data using convolutional autoencoder: Geophysics, **85**, No. 2, V119–V130.

Wang, Z., Li, B., Liu, N., Wu, B., and Zhu, X., 2020b, Distilling knowledge from an ensemble of convolutional neural networks for seismic fault detection: IEEE Geoscience and Remote Sensing Letters.

Wrona, T., Pan, I., Gawthorpe, R. L., and Fossen, H., 2018, Seismic facies analysis using machine learning: Geophysics, **83**, No. 5, O83–O95.

Wu, X., Liang, L., Shi, Y., and Fomel, S., 2019, Faultseg3d: Using synthetic data sets to train an end-to-end convolutional neural network for 3d seismic fault segmentation: Geophysics, **84**, No. 3, IM35–IM45.

Yilmaz, Ö., 2001, Seismic data analysis: Processing, inversion, and interpretation of seismic data: Society of exploration geophysicists.

Zhao, T., Jayaram, V., Roy, A., and Marfurt, K. J., 2015, A comparison of classification techniques for seismic facies recognition: Interpretation, **3**, No. 4, SAE29–SAE58.

Zheng, Y., Zhang, Q., Yusifov, A., and Shi, Y., 2019, Applications of supervised deep learning for seismic interpretation and inversion: The Leading Edge, **38**, No. 7, 526–533.